

# We are IntechOpen, the world's leading publisher of Open Access books Built by scientists, for scientists

6,900

Open access books available

186,000

International authors and editors

200M

Downloads

Our authors are among the

154

Countries delivered to

TOP 1%

most cited scientists

12.2%

Contributors from top 500 universities



WEB OF SCIENCE™

Selection of our books indexed in the Book Citation Index  
in Web of Science™ Core Collection (BKCI)

Interested in publishing with us?  
Contact [book.department@intechopen.com](mailto:book.department@intechopen.com)

Numbers displayed above are based on latest data collected.  
For more information visit [www.intechopen.com](http://www.intechopen.com)



# Mechanical Mockup of IFE Reactor Intended for the Development of Cryogenic Target Mass Production and Target Rep-Rate Delivery into the Reaction Chamber

*Irina Aleksandrova, Elena Koresheva, Evgeniy Koshelev,  
Boris Kuteev and Andrei Nikitenko*

## Abstract

Target production and its delivery into the reaction chamber of high repetition rate facilities are the most challenging issues in inertial fusion energy (IFE) research. At the Lebedev Physical Institute of Russian Academy of Sciences (LPI), efforts are underway on creation of the mechanical mockup of IFE reactor (MM-IFE) for developing the reactor-scale technologies applicable to mass production of IFE targets and their delivery with a repeatable rate into the chamber of IFE reactor. In this chapter, we discuss the current status and further trends of developments in the area of advanced target technologies underlying the research and development program on MM-IFE.

**Keywords:** inertial fusion energy, free-standing target systems, mass production, repeatable operation, noncontact delivery

## 1. Introduction

The goal of IFE research is development of high-precision and mass production technologies for fueling a commercial power plant at the rate of  $\sim 10$  Hz [1]. The conventional approach to solid layering based on the beta-layering method [2] is unable to ensure the IFE requirements, as it (a) works with targets fixed on a suspension (no repetition rate operation), (b) has a long layering time (more than 24 h that leads to a large tritium inventory), (c) shows the grain boundaries dynamic under thermal and mechanical loads in time between the moment just after target preparation and the laser shot, which results in roughening of the layer surface and may lead to implosion instabilities, and (d) has a high production cost (more than \$1000/target).

The beta-layering method can form a spherical fuel layer in a uniform thermal environment; however, it is inefficient in preventing local defects. Therefore, the

modern requirements are asking for development of structure-sensitive methods aimed at new layering techniques meeting the IFE needs. This is due to the fact that the progress in plasma implosion up to intensive fusion reactions lies in formation of a given fuel structure that must be isotropic for reaching fusion conditions.

At the LPI, the concept of a mechanical mockup of IFE reactor has been proposed [3] to develop reactor-scale technologies applicable to mass production of IFE targets at significant rates (**Figure 1**). The LPI program also includes extensive development work on creation of different designs of the hybrid accelerators for IFE target transport with levitation (noncontact acceleration systems).

The MM-IFE is a modular facility representing in essence a free-standing target (FST) transmission line (integral part of any fusion reactor) designed to produce IFE targets and to provide their noncontact delivery at the laser focus and synchronous irradiation by a laser (1–10 Hz). It consists of 3 main blocks: (1) cryogenic target factory (CTF) operating with isotropic fuel layers of 200–300  $\mu\text{m}$  thick (**Figure 1a**) [1]; (2) cryogenic IFE-target injector operating at accelerations  $<500\text{ g}$  and injection velocities  $V_{\text{inj}} \geq 200\text{ m/s}$  [4–8]; and (3) tracking systems for online characterization and control of the injected targets [9–12]. Replacement of the FST-layering module, being the main part of CTF, on the extruder of the solid fuel pellets allows developing the technologies for continuous fuel supply into magnetic fusion energy (MFE) facilities (**Figure 1b**).

Basic elements of the MM-IFE have been tested at LPI as prototypes for risk minimization at the stages of MM-IFE construction and startup. We especially highlight that moving targets are the necessary condition for realizing the repeatable target production at required rates, their mass manufacturing and noncontact delivery.

In this chapter, we discuss some challenging scientific and technological issues associated with IFE targets, the current status of the R&D program on MM-IFE, and further trends in developing the advanced IFE technologies for high-repetition rate laser facilities.

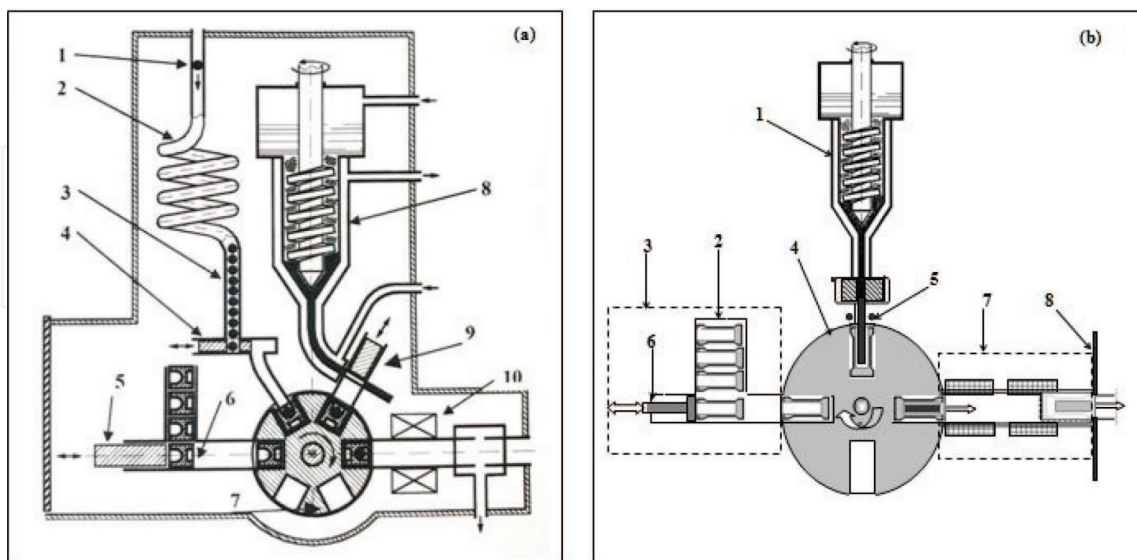


**Figure 1.** Repeatable and mass production of the fuel targets/pellets for IFE (a) and for MFE (b) reactors. In (a): 1—fuel-filled polymer shell, 2—FST-layering module, 3—cryogenic targets batch, 4—shuttle, 5—pusher, 6—target carrier (sabot), 7—drum of a revolver type, 8—extruder for protective cover production, 9—coin for the protective cover formation and delivery, 10—field coil for “sabot + target + protective cover” pull out and delivery to the start point of injector. In (b): 1—extruder of solid fuel pellets, 2—pellet carrier (sabot), made from superconductor or ferromagnetic, 3—module for sabot-repeatable delivery to the rotating drum, 4—rotating drum for rep-rate assembly of the units “sabot + pellet,” 5—heater for pellets production, 6—pusher, 7—linear electromagnetic accelerator (injector), 8—sabot brake.

## 2. Target mass production

The fuel structure is very important for the progress toward ignition. Considering the issue of high-quality cryogenic layer fabrication, we have to rely, first of all, on structural properties of hydrogen isotopes and their mixtures. Survivability of the fuel layers subjected to the environmental effects during target delivery may depend on the layer structure as well.

### 2.1 Structure-sensitive methods

Many important properties of materials are structure-sensitive, and often a relatively small number of defects have a disproportionately large effect on the material properties. Material structuring is very promising for creation of fusion materials with required properties. The role of structure-sensitive methods when developing new functional materials is especially underlined in [13]: “All materials have different chemical composition, aggregate states (solid body, liquid, and gas), allotropic modifications (graphite-diamond), or can be a mix of several substances (clay) that can be written as definition (1):

$$\begin{aligned} \text{MATERIAL} = & \\ & [\text{Chemical composition (A)} + \text{Aggregate state (A)} + \text{Allotropic modification (A)}] + \\ & [\text{Chemical composition (B)} + \text{Aggregate state (B)} + \text{Allotropic modification (B)}] + \dots \end{aligned} \quad (1)$$

However, this is obviously an inexact characteristic. The natural or introduced imperfection in the material is more important. Defects or, more generally, microstructure, define many major structure-sensitive properties of the materials. Critical for material property parameters are the type of available defects, their spatially organized packing, and interaction at multiple hierarchy levels. Chemical composition, aggregate state, and allotropic modification as a cooperative characteristic can be replaced with a more common concept “Phase.” Then, the previous definition (1) can be transformed in (2):

$$\text{Material} = \text{Phase(s)} + \text{Microstructure} \quad (2)$$

The defect structure plays an important role in determining many material properties. From technological applications, a particular interest is the mechanical and thermal characteristics. In the IFE, a practical tool for correlating the structure and properties of the hydrogen fuel is the thermal target environment; cooling rates, fuel doping, periodic mechanical influence on the target under the cryogenic layer freezing, etc. [1]. For example, depending on the cooling rates, the solid fuel layer can be in the state with a different microstructural length or grain size: isotropic ultrafine layers and anisotropic molecular crystals (real single crystals, coarse-grained crystalline). This becomes particularly important if one takes into account the properties of the hydrogen isotopes.

In the equilibrium state, the solid hydrogen isotopes consist of anisotropic molecular crystals. In our analysis, we are guided by the fact that the angular dependence of the sound velocity,  $V$ , is known for a number of substances crystallizing in the hexagonal close-packed (hcp) phase. As found in [14], the sound velocity anisotropy is inherent to hcp- $\text{H}_2$  and hcp- $\text{D}_2$  as well, and makes nearly 20% (longitudinal sound) and 33% (transverse sound). In accordance with the Debye theory, the lattice thermal conductivity is directly proportional to the value of  $V$ .



Then, even in the case of a uniform thermal environment on the target surface of the anisotropic single-crystal layers, there is a difference in the radial target temperature in time. Therefore, under uniform target heating or cooling, the normal temperature gradients onto the inner surface of such layers become different. This initiates the spherically asymmetrical sublimation (or condensation) of fuel in the target cavity and results in the layer degradation with respect to roughness and thickness.

A conventional approach to solid layering (known as beta-layering method [2]) involves crystallization from a single-seed crystal in the fixed target under extremely slow cooling ( $q \sim 3 \times 10^{-5}$  K/s) and precise cryogenic temperature control ( $<100 \mu\text{K}$ ) for obtaining the layers like a single crystal. In a uniform thermal environment, the beta-layering method can form a spherical fuel layer, but it is not efficient in preventing the local defects. The target lifetime (layer roughness is less than  $1\text{-}\mu\text{m}$  rms) is of a few seconds after reaching the desired temperature [2]. This is implication of the fact that D-T layers formed by beta-layering are obtained as a result of almost equilibrium process of the crystal growth, and all the features of the equilibrium crystalline state will be inherent in such layers, including the temperature-dependent behavior of the local defects on the inner D-T surface. Besides, the total layering time is  $\sim 24$  h or even more [2]. Thus, the beta-layering method is not efficient for mass target fabrication for IFE. It is of one-of-a-kind technique, and this is very expensive [2].

In [1], it is shown that the fuel structure dominates among the important remaining risk factors because the progress in plasma implosion up to intensive fusion reactions lies in formation of the fuel structures which must be isotropic for reaching the fusion conditions. **Figure 2** illustrates the cooling rates required to obtain isotropic fuel layers to withstand the thermal and mechanical environment during target fabrication and delivery.

### 2.2 FST layering method for high-repetition rate facilities

The LPI program on the target science and technology has recently been focused on the ability to inexpensively fabricate large quantities of targets by developing a specialized layering module of repeatable operation. The targets must be free-standing, or unmounted. At the LPI, the experience gained in the technology development based on rapid fuel layering inside moving free-standing targets (which refers to as FST layering method) can be used for creation of a next-generation FST layering module for high-repetition rate facilities. For typical shell sizes ( $1\text{--}4$  mm), the FST-layering time is very small ( $<30$  s, see Section 2.2) in comparison with the beta-layering method usually applied in the compression experiments ( $\geq 24$  h [2]).

FST layering is a structure-sensitive method to govern the fuel layer micro-structure. Such approach has been developed at LPI [1] to form an isotropic ultrafine solid fuel (submicron crystalline called “fine-grained” crystalline and nanocrystalline) which supports the fuel layer survivability under target injection

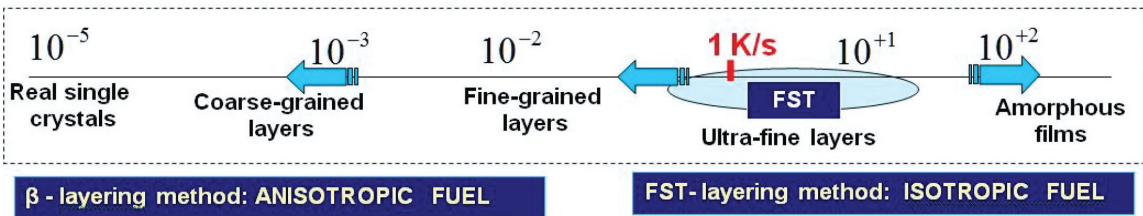


**Figure 2.**  
The fuel structure of the cryogenic layers depends on the cooling rates, and so on the layering method.

and transport through the reaction chamber. During the FST layering, two processes are mostly responsible for maintaining a uniform layer formation:

- first, during the target rolling along the spiral layering channel, the forced target rotation results in a liquid layer symmetrization;
- second, the heat transport outside the target via conduction through a small contact area between the shell wall and the wall of the layering channel (metal hollow tube helium cooled outside) results in a liquid layer freezing.

**Figures 3 and 4** show the operational scenario of the FST layering module (FST-LM):

- it works with a target batch at one time at cooling rates of  $q = 1\text{--}50\text{ K/s}$ ;
- FST layering does not require the target surface to be near to isothermal;
- targets remain unmounted (or free-standing) in each production step;
- transport process is the target injection between the basic units: shell container (SC), layering channel (LC), test chamber (TC);
- SC holds the fuel-filled shells until the beginning of the FST layering process;

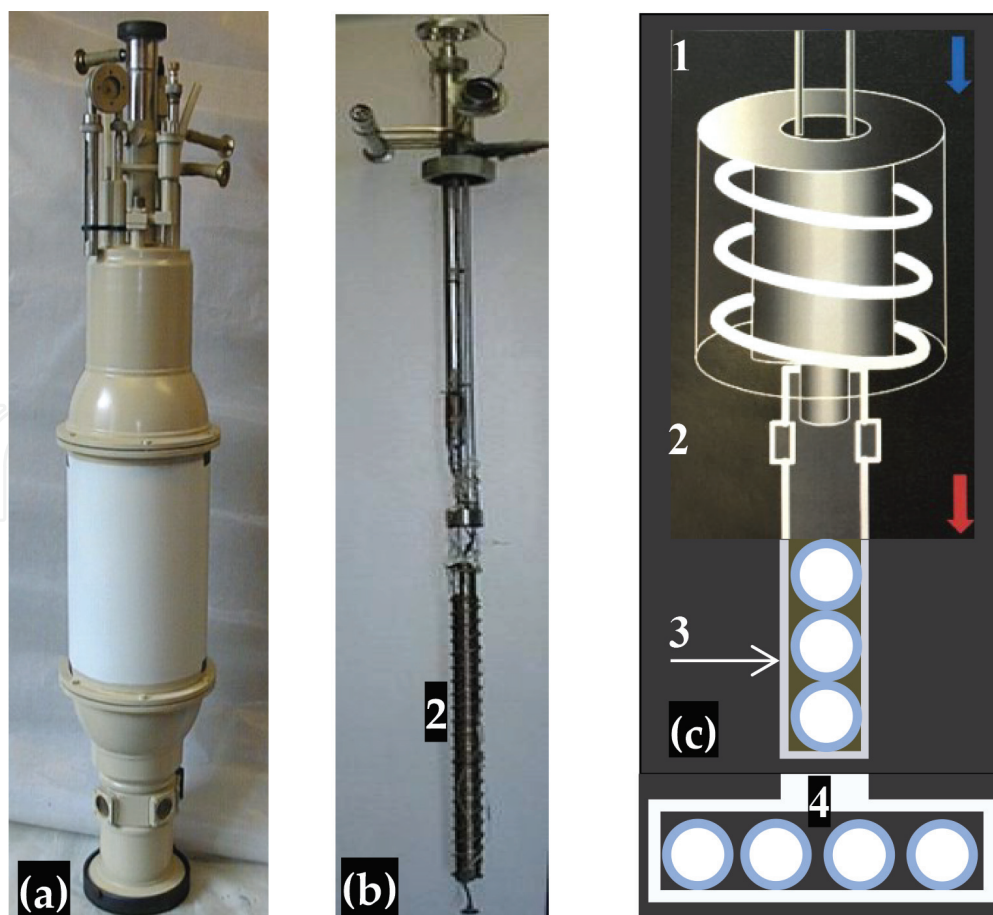


**Figure 3.**  
 FST-LM: (a) overview, (b) single spiral LC in assembly, (c) schematic of the FST-LM maintaining repeatable operation: 1—gravitation loading of the target with liquid fuel from SC to LC, 2—LC, 3—vertical target collector, 4—horizontal target collector.

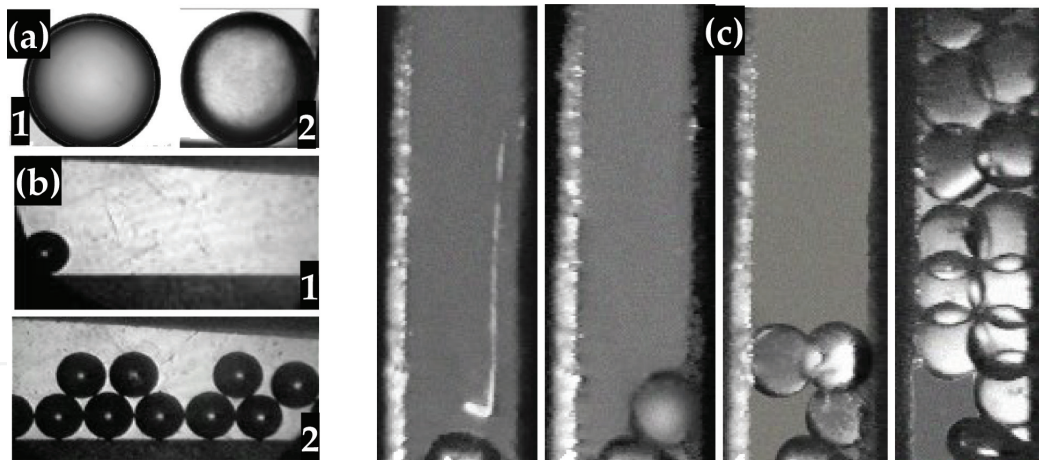


**Figure 4.**

The FST-LM operation with a rate of 0.1 Hz at  $T = 5.0$  K. In (a) FST-layering results: 1—40- $\mu\text{m}$ -thick layer ( $\text{D}_2 + 20\% \text{ Ne}$ ) in the CH shell of 1.23-mm diameter (20% Ne-additives are used for modeling  $T_2$  in the D-T fuel), 2—44- $\mu\text{m}$ -thick  $\text{H}_2$  layer with ( $\text{H}_2 + 5\% \text{ HD}$ ) in the CH shell of 1.2-mm diameter; in (b) horizontal TC: 1—1 target (0 s), 2—10 targets (100 s); in (c) vertical TC: 12 targets in 100 s.

- LC is a special insert into the layering module cryostat; it is manufactured as a spiral (cylindrical or conical);
- combined LC (CLC) is one of the most interesting cases, which consists of two spirals (acceleration spiral and deceleration spiral) in order to reduce practically to zero the target speed at the CLC output;
- TC has two types of target collectors: vertical and horizontal;
- targets move top-down in the LC in a rapid succession of one after another that allows to realize a high injection rate during finished target delivery to the TC (**Figure 3**);
- TC is a prototypical interface unit between the layering module and target injector;
- TC is currently used for finished target quality control using precise tomographic and threshold characterization.

The goal of the target characterization program is to provide reliable data in an available time. In this respect, two technologies are important: (1) fuel layering technique development (detailed information about the spatial modes, which break the target symmetry) and (2) reaction chamber fueling of a commercial power plant (targets must be injected at significant rates ( $\sim 10$  Hz) which indicates evidence of a threshold behavior of the characterization process).

The first technology requires enhancing the obtained data, and the second needs shortening the characterization time. This indicates that the process details for the characterization technology dealing with the operational times and information content are of critical importance.

A hard development work is needed to take into account the specifics of both technologies for developing a reliable characterization system to control the IFE target parameters. In the FST-LM, the reconstruction algorithms for tomographic data processing of the target layering stage are used in a hundred-projection microtomograph with a spatial resolution of 1  $\mu\text{m}$  [9, 10]. Moving target tracking is a challenge task and it is becoming increasingly important for IFE applications.



A promising way for *online* measurement of the actual position and quality of the flying target in the reaction chamber is automatic target tracking algorithm based on the Fourier holography [11, 12].

The targets' gravitational loading (one-by-one target injection) from the LM to the TCs (vertical and horizontal) with a rate of 0.1 Hz at  $T = 5$  K is shown in **Figure 4**.

Peculiarities of the FST layering process consist in the following:

1. A fundamental difference of the FST layering from the generally accepted approaches is that it works with free-standing and line-moving targets that allow starting developments on the FST transmission line of repeatable operation.
2. High cooling rates combined with high-melting additives to fuel content (**Figure 4a**) result in creation of a stable ultimate-disordered structure with a high defect density or isotropic medium (ultrafine fuel layers).
3. Additives work as stabilizing agents keeping the grain size stable and, as a consequence, keeping the thermal and mechanical stability of the ultrafine cryogenic layers.
4. For D-T mixture (having the molecular composition: 25% of  $D_2$ , 50% of DT molecules, and 25% of  $T_2$ ), just  $T_2$  is considered as a high-melting additive with respect to  $D_2$  and DT (**Figure 4**).
5. Isotropic ultrafine layers have an adequate thermal and mechanical stability for the fuel layer survivability under target injection and transport through the reaction chamber [1, 15–19].
6. An important parameter is the target lifetime within a temperature interval  $\Delta T$ , in which a stable ultrafine fuel structure can exist. Our study shows that the fuel doping in the range of  $\eta = 0.5$ –20% (neon, argon, tritium) makes this interval greatest possible, from 4.2 K right up to the temperature of fuel melting [1, 19].
7. Vibrations during FST layering are additional and effective means to meet the demands on the fuel layer formation with inherent survival features. Periodic mechanical impact on the fuel is one more option to a fuel structurization. Therefore, we plan experiments using a classical FST-LM combined with a special vibrator for launching the high-frequency waves in the top part of the LC which in turn will work as a waveguide, maintaining a vibration loading on the moving targets during their layering [1, 22].

### 2.3 FST layering time for direct-drive high-gain targets

In [15], we proposed a model for rapid fuel layering inside moving, free-standing targets. It is based on solving the Stephen's problem for moving boundaries between the fuel phases (gas, liquid, and solid) and for nonlinear boundary condition onto the outer shell surface. The heat transport through the target is conduction through a small contact area. The computational tools allow one to model the layering time as a function of the target and LC parameters and other experimental



conditions. The total layering time is typically less than 15 s (for targets less than 2 mm in size).

At the current stage of research, the FST model was adaptable and scalable for IFE targets ( $\sim 4$  mm). For comparison, in our analysis, we consider several direct-drive target designs for different laser energies  $E_L$ :

- OMEGA ( $E_L = 30$  kJ) baseline target [23]: a 0.46-mm-diameter polymer (CH) shell with a 3- $\mu$ m wall and a fuel layer of 100- $\mu$ m thick;
- High-power laser energy research (HiPER,  $E_L = 200$  kJ) baseline target (BT): the HiPER-scale targets are of two types [18]. The first one (BT-2) is a 2.094-mm-diameter CH shell with a 3- $\mu$ m wall. The solid layer thickness is 211  $\mu$ m. The second (BT-2a) consists of a 2.046-mm-diameter CH shell with a 3- $\mu$ m wall having fuel-filled CH foam (70  $\mu$ m) on its inner surface. Onto the foam, there is a 120- $\mu$ m-thick pure solid fuel;
- Classical high-gain target (CHGT,  $E_L = 1.3$  MJ KrF laser) developed by Bodner and coauthors [24]: "...a new direct-drive target design that has a predicted energy gain of 127 using a 1.3 MJ KrF laser, and a gain of 155 using 3.1 MJ." For 1.3 MJ KrF laser, the target specifications are as follows: the vapor cavity has a 1500- $\mu$ m radius. The pure D-T (190  $\mu$ m) fuel is surrounded by an ablator that consists of a CH foam ( $\sim 10$  mg/cm<sup>3</sup>) filled with frozen D-T (261  $\mu$ m). The ablator is surrounded by a 1- $\mu$ m plastic coating (polystyrene, polyimide, etc.) to contain the D-T fuel. The plastic coating is then surrounded by an overcoat of a thin high-Z material such as gold to withstand the thermal chamber environment.

**Figure 5** scales the FST layering time for cryogenic targets of a few millimeters long.

**Table 1** presents our new modeling results obtained for CHGT, which is of special interest. The FST layering time ( $\tau_{\text{form}}$ ) does not exceed 23 s for D<sub>2</sub> fuel and 30 s for D-T fuel. In order to overcome the gravitational fuel sag to the shell bottom, the FST layering uses a moving target that allows avoiding the difficulties inherent in the cryogenic layer formation in the fixed targets. The shell rotation causes a spread of liquid fuel over the inner shell surface, and under certain conditions (sufficient value of  $\tau_{\text{liquid}}$ ), it results in a uniform layer formation. This important effect makes topical to study a dynamical spread of the liquid fuel inside the moving target and to develop numerical models of the process. The obtained results (theoretical and experimental) can be found in [10, 15].

Thus, for dynamical fuel symmetrization in a batch of rolling targets (**Figure 3**), the time of liquid phase existence,  $\tau_{\text{liquid}}$ , is a key parameter and must be sufficient for a cryogenic layer symmetrization. This depends on a temperature  $T_{\text{in}}$  of the target entry in the LC (initial target temperature before FST layering). Decrease in temperature  $T_{\text{in}}$  will lead to decrease in the total layering time at the expense of  $\tau_{\text{liquid}}$  (**Table 1**). Therefore, when designing the FST-LM for CHGT, it is essential to manage the value of  $T_{\text{in}}$  in a way that limits the risks and achieves maximum possible growth of  $\tau_{\text{liquid}}$ .

In near-term plans, we consider the approach based on the FST layering method as a credible path for creating a repeatable operating FST supply system (FST-SS). The first step in this direction is the development of the next-generation FST-LM for high-gain direct-drive targets, which are the shells of  $\sim 4$  mm in diameter with the shell wall of different designs from compact and porous polymers. The layer thickness is  $\sim 200$   $\mu$ m for pure solid fuel and  $\sim 300$   $\mu$ m for in-porous solid fuel. Most

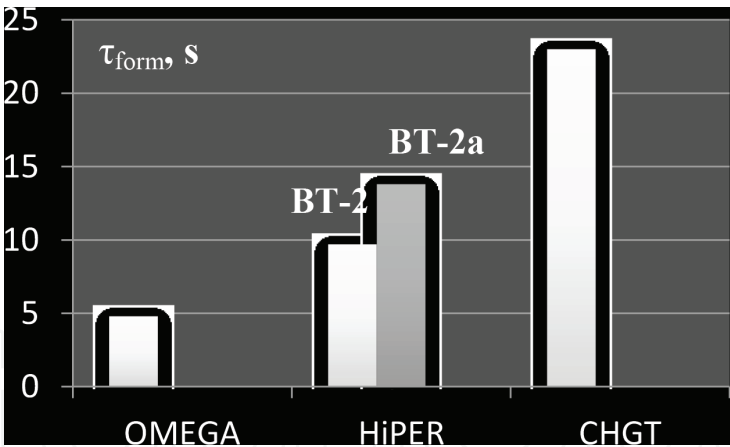


**Figure 5.** The FST layering time for several direct-drive target designs was calculated using the computational codes developed at LPI [15].

D <sub>2</sub> fuel			D-T fuel		
T <sub>in</sub> (K)	τ <sub>liquid</sub> (s)	τ <sub>form</sub> (s)	T <sub>in</sub> (K)	τ <sub>liquid</sub> (s)	τ <sub>form</sub> (s)
35.0	17.48	22.45	37.5	22.14	28.52
27.5	7.08	12.05	28.0	7.87	14.25

**Table 1.** FST layering time for CHGT.

of the theoretical efforts have focused on the development of computational models of the IFE target response during FST-formation cycle [1]: fuel filling–fuel layering–target injection. Using the codes allows planning experiments and studying the behavior of these targets in the FST-LM.

Current status of the FST technologies underlies the future research that focuses on the FST-LM prototype development, challenges and advances in IFE target fabrication. We use the CHGT to design a high rep-rate FST-LM and analyze recent experiments with different LCs. Our experiments were made with the mockups of different designs, and the required LC geometry was found. The time-integral performance criterion is that the target residence time  $t_{res}$  in the LC must be more than the fuel layering time  $\tau_{form}$ . **Figure 6** shows three mockups: mockup 1 M-1 (one-fold spiral),  $t_{res} = 9.8 \pm 0.5$  s; mockup 2 M-1 (two-fold spiral),  $t_{res} = 23.5 \pm 1.7$  s; mockup 3 M-2 (three-fold spiral),  $t_{res} = 35.0 \pm 2.0$  s.

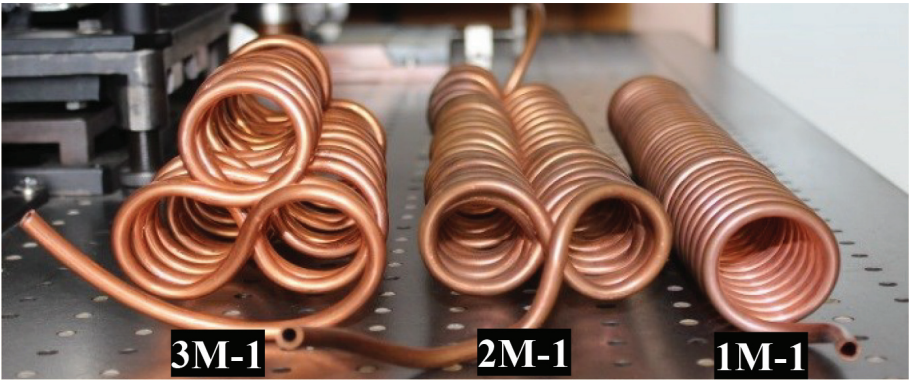


**Figure 6.** Different LC mockups which are planned to be used in the FST-LM to promote development of effective affordable technology alternatives.

These measurements show that 4-mm targets can be manufactured by the FST layering method using  $n$ -fold-spiral LCs at  $n = 2, 3$ , because they maintain the gain in time of the target residence in the LC and in fuel layer symmetrization during target rolling. Note that currently only curved LCs in a specialized geometry and moving targets are successful for developing the FST-LM of repeatable operation, which works with a target batch rolling along the LC.

Our latest effort underlies the future research on creation of the FST-LM as a means of a steady-state target-producing device, which is compatible with a noncontact schedule of the target delivery to the reaction chamber.

### 3. Target repeatable delivery

During the target delivery, it is necessary to maintain the fuel layer quality in the process of target acceleration and injection. For this reason, the target must be placed into a special target carrier (sabot). Using sabots, there occur some contact problems. Because of a tight seal between the sabot and the barrel, any damage of the barrel and the sabot surface will affect the injector performance and sabot reusing.

Recently, we have started the investigation into magnetic levitation as an alternative technology of noncontact manipulation, positioning and transport of the finished cryogenic targets. From the moment of discovery of bulk high-temperature superconductors (HTSC), which can stably levitate above the permanent magnets, the magnetic levitation (maglev) transport systems are of great interest for their potential application. The transport process with levitation results from the direct use of the diamagnetic characteristics of the HTSC materials. Their unique features can be exploited in the process of levitation and guidance of a HTSC-sabot as well.

In IFE research, this approach attracts a significant interest due to maglev potential for almost frictionless motion. The challenging scientific and technological issues associated with this task are being addressed through a combination of material selections and material property measurements, mathematical and experimental modeling, demonstration of the HTSC-sabot acceleration in laboratory-scale tests.

#### 3.1 Noncontact acceleration system

A noncontact acceleration system proposed at the LPI is a combination of three basic elements: (1) electromagnetic acceleration system (EM-AC), which includes the field coils generating the traveling magnetic waves, (2) levitation system (permanent magnet guideway or PMG), which includes a magnetic rail (or magnetic track), and (3) sabot including several HTSC components. **Figure 7** illustrates the operational principle of the system. During acceleration, the target is protected with a levitating HTSC-sabot, and the diameter of the barrel exceeds the sabot diameter. This is a small-scale prototype under construction of a hybrid accelerator “EM-AC + PMG” at the LPI. The concept of “EM-AC + PMG” is completed and the proof-of-principle (POP) experiments have confirmed the benefits of this approach.

The prove-of-principle (POP) experiments (**Figure 8**) on magnetic acceleration of the levitating HTSC-sabot are made in the mutually normal magnetic fields: the first is **B1** (from the field coil to move the HTSC-sabot) directed along the acceleration length and the second is **B2** (from the permanent magnets to counteract the gravity) directed normally to the acceleration length (**Figure 7c**). The Meissner effect [25] dictates that both magnetic fields generate the surface currents around the superconductor (in our case, it is the HTSC-sabot) in corresponding



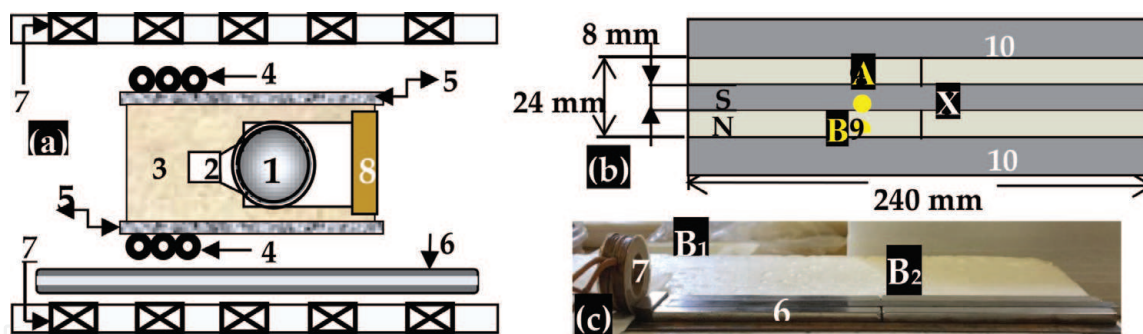


**Figure 7.** Schematic of “EM-AC + PMG”. In (a): 1—target, 2—conical support of the target nest, 3—sabot matrix (polymer), 4—HTSC-coils (driving body based on superconducting MgB<sub>2</sub>-cables), 5—HTSC-plates for providing a stable levitation along the magnetic track, 6—magnetic track, 7—field coils, 8—protective cover; in (b) and (c): parameters and a side view of the experimental setup with directions of the driving force **B**<sub>1</sub> and the levitation force **B**<sub>2</sub> (9—ferromagnetics, 10—permanent magnets).

directions that leads to its simultaneous acceleration and levitation (simultaneous presence of the driving force along the vector **B**<sub>1</sub> and of the levitation force along the vector **B**<sub>2</sub>).

The experiments were conducted under the following conditions.

- To ensure the successful acceleration, the field coil and HTSC-sabot are fixed over the magnetic track of the PMG-system so that the horizontal axis of the coil and the HTSC-sabot coincide (**Figure 8b**).
- The HTSC-sabot motion has been driven by the electromagnetic pulse generated by the field coil, that is, by using a running gradient of the magnetic induction (accelerating running pulse, or ARP).
- As the HTSCs are diamagnetic, the HTSC-sabot is pushed out from the area of a stronger magnetic field.
- The starting parameters of the coil pulse: the pulse duration is 1 ms, the current amplitude is 200 A, the maximum magnetic induction is 0.35 T.
- The temperature in the experiments was  $T = 80$  K for the following reason. Our previous studies have demonstrated a high efficiency of “HTSC-PMG” interaction in a wide temperature range  $\Delta T = 5\text{--}80$  K [4]. Consequently, it is possible to study the HTSC-sabot acceleration at temperatures close to 80 K, that is, under the nitrogen cryogenics. This is especially important because it

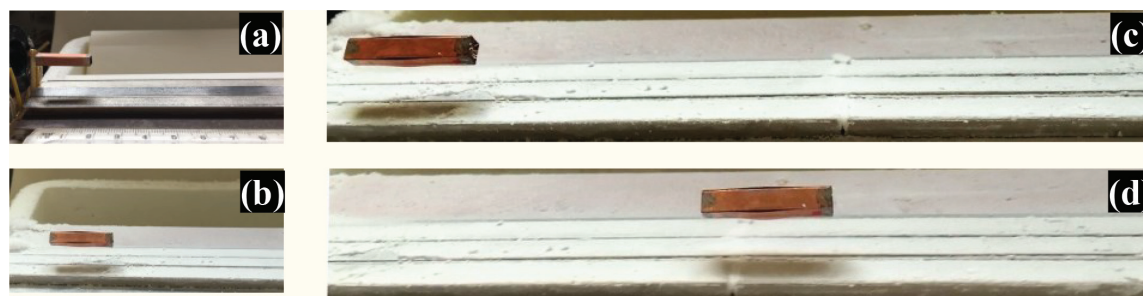


**Figure 8.** HTSC-sabot friction-free acceleration by the driving electromagnetic pulse generated by the field coil ( $T = 80$  K). In (a): HTSC-sabot before acceleration; in (b) HTSC-sabot starts motion, in (c) and (d): in-time development of the acceleration process (the gap between the HTSC-sabot and the magnetic track is keeping unvarying with time).



allows the acceleration experiments to be feasible at  $T \sim 80$  K taking into account that such experiments at  $T \sim 18$  K are unpractical inside a small test chamber of the cryostat.

**Figure 8** shows the results of the demonstration tests: a set of freeze-frame shots of the acceleration process of the levitating HTSC-sabot at  $T = 80$  K using the linear PMG-system.

The HTSC-sabot is trapped (**Figure 8a**) and accelerated in front of a magnetic traveling wave (**Figure 8b–d**). It reaches a velocity of 1 m/s and keeps this velocity on all sabot-track length of 22.5 cm (motion time is  $t = 0.22$  s). The levitating drift is not observed. Technologically, this allows a convenient spacing of the multiple coils (also called a multiple-stage accelerator, **Figure 7a**), and leads to realizing very high velocities of the HTSC-sabot. It is necessary to highlight that in the experiments, we did not use a special driving body, and the obtained result of 1 m/s is due to the surface currents in the HTSC material itself arising from the magnetic field  $B_1$  generated by the field coil.

Thus, a friction-free HTSC-sabot transport can be realized with the levitation devices using superconductors and permanent magnets. The continuous space range of the stable position of the levitated HTSC-sabot has been demonstrated by the experimental results. Features of the device concepts and their future applications in the noncontact delivery system are discussed below.

### 3.2 HTSC materials

Generally, superconducting material selection for sabot manufacturing is defined, first of all, by the temperature requirement for IFE targets which must be at  $T = 18.3$  K [1–3]. Superconductors are classified into two types [25], called type-I and type-II, based on their diamagnetic properties (magnetic susceptibility  $\chi < 0$ ). Type-I superconductors (low-temperature superconductors) are in the state which is called “perfect diamagnetism” (the Meissner effect at which the magnetic lines bend around the superconductors). As the applied magnetic field increases, so does the opposing magnetization until the field reaches the critical field  $B_C$ , whereupon the superconductivity disappears. Since the type-I superconductors have the critical temperature  $T_C < 10$  K (i.e., their heating above 10 K destroys their superconductivity), they cannot be considered as candidates when developing a maglev transport system for application to IFE. Besides, type-I superconductors typically have the critical field values too low for practical applications.

In the study, we use the samples from HTSCs, which are known to be type-II superconductors. They have two values of the critical magnetic field  $B_C$  (called first  $B_{C1}$  and second  $B_{C2}$ ). Below  $B_{C1}$ , type-II behaves similar to the type-I. When the applied magnetic field is between  $B_{C1}$  and  $B_{C2}$ , the magnetic field penetrates the type-II superconductors in the form of quantized magnetic flux lines (either tube or vortices), and they become a mixture of the normal and superconducting states. Emphasize that inside each magnetic flux tube, superconductivity is locally destroyed. Such materials can be subjected to much higher external magnetic fields and remain superconducting. This property is used for obtaining strong magnetic fields under the conditions of no thermal losses when the high currents are passing through HTSCs. In addition, the HTSC materials with critical temperatures in the range of 90–120 K have received a great deal of attention because they can be maintained in the superconducting state with liquid nitrogen (77 K).

The second issue under superconducting material selection is structural characteristics of HTSCs, which influence on the potentialities of their levitation properties. The authors of [13] revealed many interesting features related to this problem.

Different HTSC materials can have different microstructures, from so-called “superconducting glass” (superconducting ceramics) to microstructures like a type of “mosaic” with macro-, meso-, and microlevels of material ordering. This creates favorable conditions for obtaining an optimal HTSC microstructure just for taking into account the design specifics of a noncontact delivery system intended for the IFE experiments.

At the same time, it is necessary to note one more important feature related to type-II superconductors. It is a flux (or vortex) pinning. Vortex pinning results from spatial imperfections (or defects) in the material that produces local reductions of the free energy of a flux line [25], thus attracting and holding vortices to these locations. In many respects, the basic magneto-mechanical phenomenon responsible for levitation is a result of the magnetic flux pinning inherent in the interaction between a magnet and a type-II superconductor. In the mixed state, the flux lines interact with different defects and may become pinned to them (frozen in the bulk superconductor). Such defects (e.g., crystal lattice defects, grain boundaries, twin planes, stacking faults, etc.) always exist in real superconducting materials. They could work as pinning centers (including pinning by surface roughness or at a step-like surface relief), avoiding the vortex motion and consequently the energy dissipation. A vortex state looks like a “frozen” in the superconducting material, and any spatial motion of the superconductor will cause the flux tubes to move. In order to prevent that, the superconductor remains “trapped” in its original state (be it levitating at the fixed point or under motion along a magnetic track).

Thus, the bulk of type-II, HTSC materials breaks down into two regions: superconductive—from which the external field is completely expelled, and normal—through which the external field penetrates. The diamagnetic characteristics of the material are more or less pronounced depending on its “degree of superconductivity.” These features can be exploited in the process of HTSC-sabot levitation and guidance. Therefore, the superconducting material science and technology is of critical importance. Currently, there are many structural efforts to enhance the pinning properties in HTSCs by creating structural defects in them using different techniques. These structural defects can be in the form of periodic pinning arrays or random pinning distributions (i.e., with different ordering states of a vortex lattice) to improve the maglev properties of the HTSCs.

In our experiments, the HTSCs are superconducting ceramics based on  $\text{YBa}_2\text{Cu}_3\text{O}_{7-x}$  (or Y123; production of LPI) and superconducting tapes of second generation (2G HTSC) based on  $\text{GdBa}_2\text{Cu}_3\text{O}_{7-x}$  (or Gd123; production of SuperOx, Ltd.). The obtained results have shown that these HTSCs can be successfully used to maintain a friction-free motion of the HTSC-sabots, and also to provide a required stability of the levitation height over the whole acceleration length due to the pinning effect. This becomes more viable because the critical temperature of Gd123 and Y123 is  $T_c \sim 90$  K, which is nearing the boiling point of nitrogen (**Table 2**).

The HTSC-sabot designs were in the form of an “open parallelepiped” (its cross section forms a trough) or in the form of a “hollow parallelepiped” (its cross section forms a square).

HTSCs	Density ( $\rho$ , g/cm <sup>3</sup> )	$B_C$ at 0 K (T)	$T_C$ (K)
Y123 [4, 6]	4.33	>45	91
Gd123 [5, 26]	3.25	> 45	92

**Table 2.**  
*Parameters of the HTSC materials used in the experiments.*

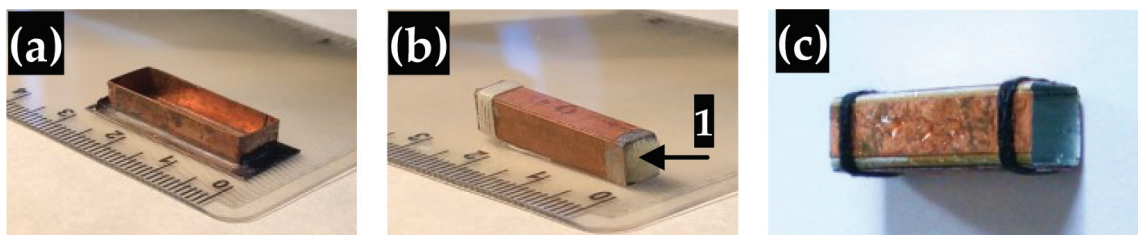


**Figure 9.**

*Usual HTSC-sabot designs used in the experiments. In (a): “open parallelepiped” (model#1); in (b): “hollow parallelepiped” (model#2 + polymer foam (1)); in (c): model#3—“hollow parallelepiped” (empty).*

Here, we set the task of accelerating different HTSC-sabots (**Figure 9**) over different PMG-systems to study the stability of the main levitation parameters: the load capacity (mass of an object which HTSC-sabot can maintain), the space locking (three-dimensional stability of HTSC-sabot), and the gap between the HTSC-sabot and the magnetic track (levitating drift). The HTSC-sabot parameters are as follows:

- Model #1, “open parallelepiped”: Gd123 tape thickness is 0.5 mm, length inside is 25 mm, width inside is 8 mm, height is 4 mm, total mass is 1.26 g;
- Model #2, “hollow parallelepiped”: Gd123 tape thickness is 0.3 mm, internal sizes are  $4 \times 4 \times 24 \text{ mm}^3$ , total mass is 0.97 g (together with filling of polymer foam which mass is 0.38 g);
- Model #3, “hollow parallelepiped”: Gd123 tape thickness is 0.3 mm, internal sizes are  $4 \times 4 \times 30 \text{ mm}^3$ , total mass is 0.59 g (no polymer filling).

In the experiments, the force  $F$  driving the diamagnetic Gd123-tapes is given by [27]:

$$F = \frac{\chi}{2\mu_0} V_s \frac{dB_x^2}{dx}, \quad (3)$$

where  $\mu_0$  is the permeability of vacuum,  $V_s$  is the superconductor volume,  $x$  is the acceleration axis,  $\mathbf{B}$  is the magnetic induction produced by the field coil (in our case  $\mathbf{B}_1$ ). Since for diamagnetic  $\chi < 0$ , then this force is contrariwise to the gradient of the magnetic induction in the  $x$ -direction. Therefore, the HTSC-sabot is pushed out from the area of a stronger magnetic field that defines its behavior in the PMG-systems.

### 3.3 PMG-systems

The characteristics of the permanent magnets composing the PMGs are very important for their performance in terms of levitation force and stability. The PMG-systems of different configuration were used in the experiments (**Figures 8, 11–14**). Our goal was to demonstrate not only the levitation stability of the HTSC-sabots, but also their transport over the PMGs with a guidance force resulting in either linear or circular motion in a “tight space.”

The PMGs [4, 5] were constructed on the basis of neodymium permanent magnets with an axial magnetization (MIDORA, Ltd.). A magnetometer with a sensitivity of 280 mV/T was applied with the following performance data: the



positioning accuracy of a sensitive element is 0.1 mm, the measuring range is +1 T, and the absolute error is +0.005 T. The maximum magnetic induction (0.33 T right at the track's surface) was for the linear PMG (**Figure 11**) along the acceleration direction OX for a magnetic track of 24-cm long.

Note that the PMG optimization is the most critical problem of practical interest since it serves as a continuous magnetic track to generate the required magnetic field by rare-earth permanent magnets (made from an alloy of neodymium, iron, and boron to form the  $\text{Nd}_2\text{Fe}_{14}\text{B}$ ) and inserts of soft magnetic (ferromagnetic). Therefore, a feasibility study of the key technical issues such as influence of the PMG-fields of different configurations on the mechanical and timing performances of the HTSC transport process and active guidance due to different driving pulses (mechanical and electromagnetic) are under way.

In this chapter, we present an analysis of dynamic behavior for two proposed PMGs consisting of different arrangements of the permanent magnets (different shape and size). The levitation experiments in specifically designed configurations (**Figure 10**) with strongly pinned superconductors (Gd123 and Y123) display a repeatable PMG operation, allowing a simultaneous demonstration of linear and lateral stability. We have also studied the issues of how the geometrical and loading characteristics of the HTSC-sabots can affect their levitation capability at different constraints of the PMG cross section.

The main idea in the PMG construction is that the magnetic track must allow the HTSC-sabots to move freely only in one direction in order to avoid any contact with a stronger magnetic field, which pushes out them and return them to their initial trajectory (according to the Eq. (3)). This is due to the fact that any spatial motion of the HTSCs will cause the magnetic flux tubes to move. A reasonable plan to prevent this effect in the lateral direction is to make the linear PMG with the magnet poles aligned antiparallel to each other (N-S-N) for producing a considerably strong gradient for a side-to-side motion (**Figures 7, 8, 10a**). The circular PMG consists of a disk of NdFeB permanent magnet (OD = 100 mm, ID = 50 mm, 5 mm thick) embedded in the soft ferromagnetic holder to realize a required distribution of the magnetic field along the width of the magnetic track (**Figure 10b**). Since the flux tubes are magnetic fields frozen in the superconducting material, the very superconducting material itself creates a force to inhibit any motion in relation to the magnetic field, and the HTSC-sabot remains “trapped” in its trajectory. This is an efficient scheme for optimizing the levitation and guidance forces which is considered as a base to perform the search of an optimal PMG.

We have found that not only the linear PMG-systems (**Figures 8 and 10a**) but also the circular ones are promising candidates aimed at development of HTSC-maglev transport system for high-velocity target applications, target trajectory correction, and creation of a precise injector. The circular PMG testing under a typical optimization of the levitation stability has proven its robustness and efficiency. **Figure 11** demonstrates the HTSC-sabot motion with different velocities over the circular PMG shown in **Figure 10b**. In the experiments, we use a mechanical

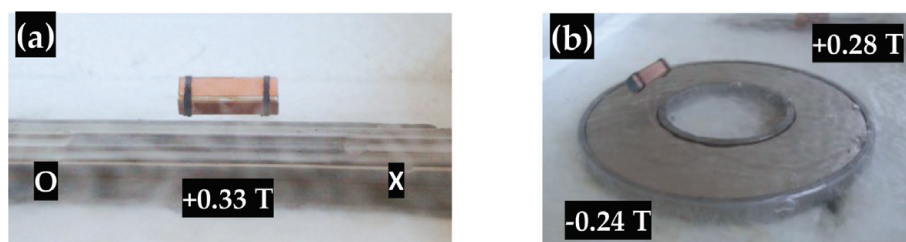


**Figure 10.**  
Acceleration of the HTSC-sabot (model #3, **Figure 9c**) over the linear (a) and circular (b) PMGs at  $T = 80\text{ K}$ .



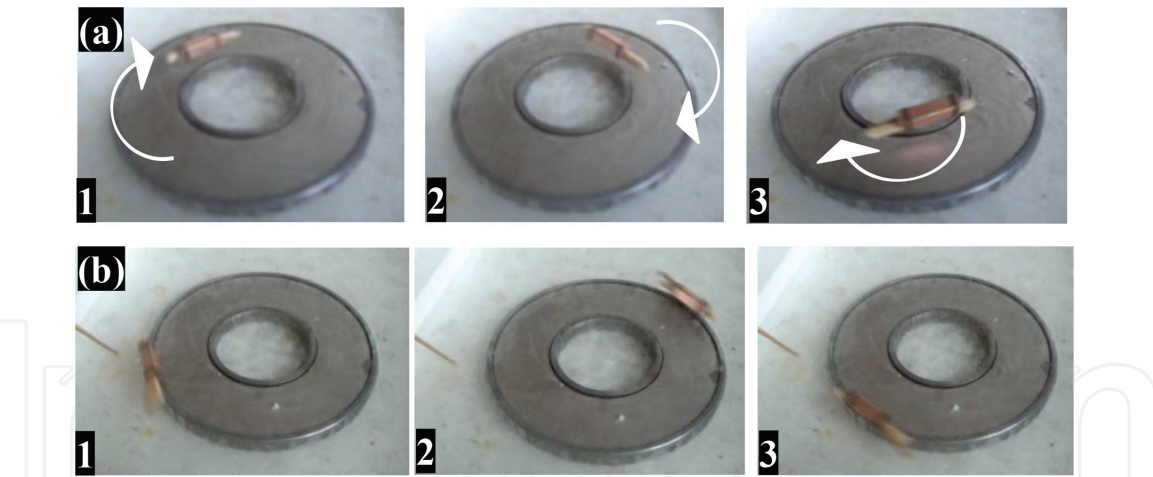


**Figure 11.**  
*Different velocities of the HTSC-sabot (model #3, load capacity: a piece of wood) over the circular PMG at  $T = 80$  K. In (a): internal orbit; in (b): external orbit.*

driving pulse to simply change the initial conditions related to placing the HTSC-sabot on different trajectories. The findings accessible from these experiments are the bases to provide the conditions when the HTSC-sabot can be accelerated in a stable orbit under different load capacities, which is directly related to the safe operation and design of the whole system. Below, we present the experimental results obtained in this area. **Figures 12 and 13** show a stable acceleration of HTSC-sabot (Model #1) over the linear and circular PMGs with several samples surrogating both spherical and cylindrical targets.

In both cases, after being disturbed during motion, the HTSC-sabot has a disturbance-induced velocity that, in general, can result in changes in the levitation and guidance forces and can cause some serious malfunctions. If these induced



**Figure 12.**  
*Acceleration of the HTSC-sabot over a linear PMG at  $T = 80$  K. In (a): HTSC-sabot moves along the magnetic track; in (b): 1—HTSC-sabot is on the middle of the track, 2—HTSC-sabot exit out of the track (load capacity: 5 spherical targets of 0.6 mg each).*

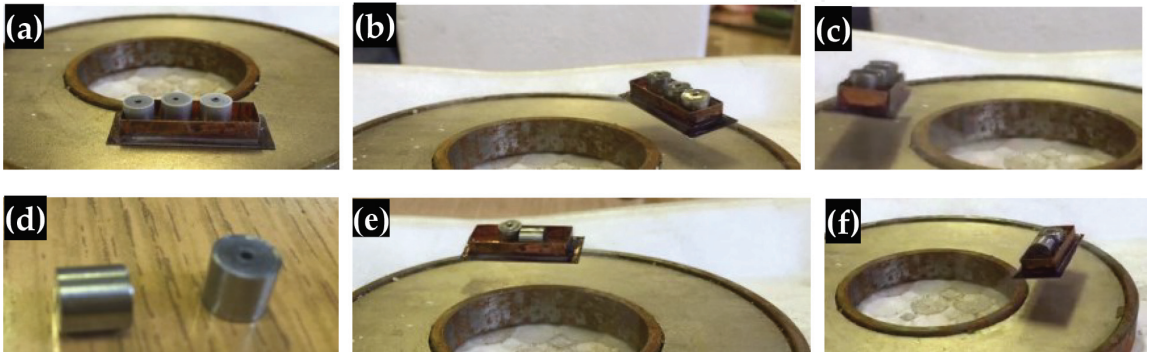


**Figure 13.**  
*Acceleration of the HTSC-sabot over the circular PMG at  $T = 80$  K. In (a): before acceleration; in (b) and (c): during acceleration (load capacity: three cylindrical targets of 1.1 g each); in (d): before acceleration; in (e) and (f): during acceleration (load capacity: two cylindrical targets of 1.1 g each are placed in the same HTSC-sabot in such a way that one of them is vertical, and the other is horizontal).*

external disturbances are considerable, vertical and lateral displacements of the levitating body may occur simultaneously. In this connection, it was very important to study the levitation stability of the HTSC-sabots.

Our findings (**Figures 8, 10–13**) have shown that a basic phenomenon responsible for the levitation stability is the flux pinning effect inherent in the interaction between a type-II superconductor and a permanent magnet. For specifically designed configurations of PMGs (peculiar distribution of the magnetic field), the flux-pinning is tending to enhance the stability of HTSC-sabot levitation, and strongly pinned superconductors (Gd123) display high stability, allowing the demonstration of striking effects, such as vertical, lateral, or inverted levitation. They look like they are pinned to a magnetic track so they can stably levitate over permanent magnets without any active control. Thus, the HTSCs can be designed to enhance the effect called “enhanced flux pinning.” It is of a great importance for target trajectory correction during its delivery inside the assembly of “HTSC-sabot + target.” Several remarks should be made here.

An idea of using the magnetic field to control the “HTSC-sabot + target” transport is very attractive for the following reasons. In HTSC-maglev, the stable transport with levitation is caused by a combination of the Meissner effect (quantum levitation) and the flux pinning in HTSCs (quantum locking).

As it is mentioned above, in HTSCs the magnetic field is not excluded completely, and the superconductor tries to keep the magnetic flux or vortices pinned in weak areas (e.g., grain boundaries or other defects). Energetically, this means that the vortices favor to be located in the bulk of HTSCs where defects exist. Any spatial displacement of the HTSCs causes the magnetic flux motion. Using the vortex physics [26] under the PMG construction, we have succeeded in controlling the magnetic field so that there are some directions where the HTSC-sabots can move, and there are some directions where the HTSC-sabots remain “trapped” (located in a “tight space”).

Along the magnetic track (or acceleration length, both linear and circular), there are no magnetic field changes, which allows the HTSC-sabots to move forth and back with no energy loss. Normal to the acceleration length, the magnet poles are aligned antiparallel to each other (N-S-N, see, for example, **Figure 7b**) that produces a considerably strong gradient along the width of the magnetic track. This gradient prevents the motion of HTSC-sabots, and they remain located in the transverse direction. In other words: (1) flux-pinning makes the HTSC-sabot motion trapped in the space within a PMG field; (2) flux-pinning makes the HTSC-sabot orientation fixed in the space so that they will not reorient themselves without any external action (so-called a three-dimensional locking of type-II superconductors). This process of locking by height and orientation reduces any undesirable wobble during HTSC-sabot movement. Thus, the obtained results indicate that we have an effective set of tools (quantum levitation and quantum locking) for a noncontact acceleration of the HTSC-sabots in the mutually normal magnetic fields generated by the field coil and the PMG-system.

### 3.4 HTSC-sabot design

The HTSC-sabot design is a vital point in the process of its transport with levitation. The most striking examples are the HTSC-sabots, the shape of which corresponds to Model #4 and Model #5 (**Figure 14**):

- Model #4, “hollow parallelepiped + 5 wings”: Gd123 tape thickness is 0.3 mm, Model #2 ( $4 \times 4 \times 30 \text{ mm}^3$ ) + 5 wings ( $12 \times 12 \text{ mm}^2$ ), total mass is 1.46 g.

- Model #5, “hollow parallelepiped + 5 wings” on a Gd123 tape ( $35 \times 12 \times 0.3 \text{ mm}^3$ ): total mass is 1.97 g.

Nevertheless, **Figure 15a** shows that the Model #4 (the Model #2 in assembly with five wings) as an independent target carrier is inefficient. The wings keep the Model #4 “nonlevitated” so that it comes into contact with the magnetic track. However, if using the same Model #5 (the Model #4 placed on a superconducting Gd123 tape), the levitation effect occurs again (**Figure 15b**), because the Model #5 is a combination of the levitating Gd123 tape and the Model #4 as a load capacity.

These results can be explained by a special mapping of the magnetic lines which are bending around the Model #4 creating the magnetic field close to the second critical value,  $B_{C2}$ , or even more this value ( $T = 80 \text{ K}$  is close to  $T_C = 92 \text{ K}$ ). At a step-like surface relief (critical bending of the magnetic lines), the magnetic field is able to considerably slip through the HTSC material of the Model #4, and the normal cores of vortices begin to adjoin and then the volume superconductivity disappears. In other words, under roughening of a surface, the number of vortices becomes so numerous that there is no space left for superconductivity, and the superconducting material becomes less and less diamagnetic.

### 3.5 HTSC-driving body

The driving body is a component of the HTSC-sabot (**Figure 7**). In our study, we consider a superconductor on the basis of  $\text{MgB}_2$ -cables because of its potential for applications at high magnetic field [28, 29]. However, under using  $\text{MgB}_2$ -driving

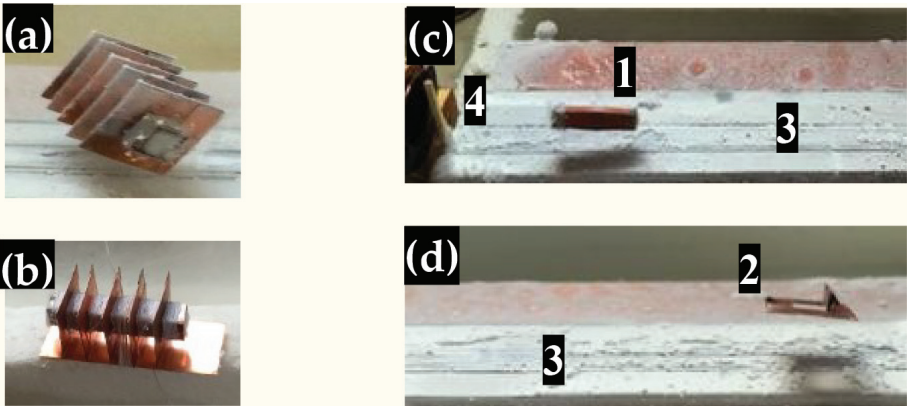


**Figure 14.** HTSC-sabots with several detached wings. In (a) and (b): overview of model #4 and model #5; in (c) and (d): acceleration ( $T = 80 \text{ K}$ ) of the different components of model #4 (1—hollow parallelepiped, 2—wing) along the magnetic track 3 by the field coil 4.

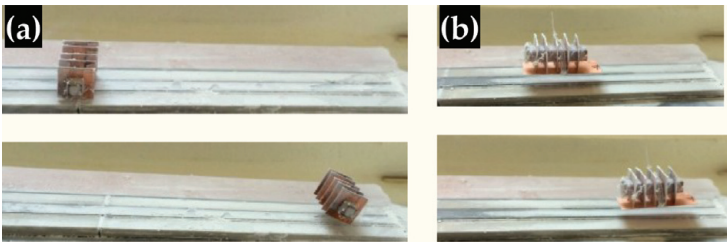


**Figure 15.** Levitation of the model #4 and model #5 at  $T = 80 \text{ K}$ . In (a): lack of levitation for the model #4 (its motion is caused by a magnetic track inclination, that is, by gravity under the inclination angle less than  $10^\circ$ ); in (b): the same HTSC-sabot (model #4) levitates just on a Gd123 tape (i.e., model #5 levitates stably).



body, the acceleration parameters which are of interest for IFE (injection velocity  $V_{inj} = 200$  m/s) become unsuitable for the laboratory-scale tests. Therefore, the POP experiments (**Figure 8**) have been carried out with HTSC-sabots (Gd123) without any  $MgB_2$ -coils in their design. The HTSC-sabot (Model #2) is accelerated using the magnetic field **B1** generated by the field coil (ARP). The acceleration process maintenance is caused by the surface currents induced in the bulk Gd123 itself due to ARP, which results in arising the driving force along the acceleration length. The HTSC-sabot obtains a velocity of 1 m/s and keeps it over the whole magnetic track (22.5 cm). This is a demonstration of the one-stage accelerator.

Below, we discuss the issue related to a multiple-stage accelerator. The first problem is as follows: what characteristics of  $MgB_2$ -cables are required to reach the required lower limit on the injection velocity  $V_{inj} = 200$  m/s. We list below some distinguish features of  $MgB_2$ , which are important for our study [28, 29]:

- $MgB_2$  critical temperature is  $T_C = 39$  K, which is twice above than for  $Nb_3Sn$ , and four times above than for  $Nb-Ti$ ;
- $MgB_2$  is a promising superconductor for applications in the temperature range 15–20 K which meets the temperature tolerance for the IFE targets which must be at  $T = 18.3$  K before the laser shot to obtain the maximum energy yield from the fusion reaction [1–3];
- $MgB_2$  possesses high values of the critical current at a rather small sensitivity to intergranular contacts;
- simple chemical composition and low cost of the initial components for its synthesis;
- achievement of typical magnetic fields more than 1.5–2.0 T at lower capital investments and at lower cost of commercial operation;
- stability of  $MgB_2$  characteristics under the conditions of radiative environment;
- due to a weak anisotropy of the critical properties, the  $MgB_2$ -cables can be well-shaped that is of a great importance for optimizing the current density in superconducting coils. Besides, the  $MgB_2$ -cables can be of round or rectangular cross section and have a small weight. These are most important parameters for practical applications of  $MgB_2$ -cables in the HTSC-sabot design.

For estimations of the acceleration length,  $L_a$ , for a multiple-stage accelerator with a superconducting driving body (in our case  $MgB_2$ -cables), we use the following relation [8]:

$$L_a = \frac{\pi}{2} \cdot V_{inj}^2 \cdot \frac{R_{FC}}{R_{SC}} \cdot \frac{M_{sab}}{F_{pin} V_S}, F_{pin} = J_C(B_0, T_S) \cdot B_0, \quad (4)$$

where  $M_{sab}$  is the mass of the “HTSC-sabot + target” assembly,  $R_{FC}$  is the field coil radius,  $R_{SC}$  is the radius of the superconducting coils ( $R_{FC}/R_{SC} = 5$ ),  $F_{pin}$  is the pinning force density,  $J_C$  is the critical current density, which depends on the magnetic induction in the coil center  $B_0$  and superconductor temperature  $T_S$ . The value of  $J_C$  (defined as the current density where the pinning force and the Lorentz force become equal) determines the onset of resistivity [28–30]. In (4), a difficulty arises in calculation of  $L_a$  because only knowing the relationship between  $J_C$  and  $B_0$ ,



External field (T) [30]	1	0.5	0.25
Critical current (A) [30]	2500	4000	5000
Sabot acceleration (g)	800	640	400
Acceleration length (m)	2.5	3.125	5.0

**Table 3.**  
*MgB<sub>2</sub>-driving body acceleration efficiency at  $T_S = 20$  K.*

the pinning force density  $F_{pin}$  can be found for the superconducting coils proposed for the sabot acceleration. For MgB<sub>2</sub>-cables of 1.18 mm in diameter, the critical current vs. the magnetic field at temperatures of 4.2, 9.8, 15, 20, and 25 K was measured in [30]. Using these data, we have made the calculations under the actual operating conditions: (a) the target design is CHGT, and its mass is 5 mg (see Section 2.2); (b) the HTSC-sabot is “open parallelepiped” to exclude a bend of the Gd123 tapes (see Section 3.2); and (c) the mass of the assembly “HTSC-sabot- + CHGT” is 0.5 g. The calculation results are presented in **Table 3**.

Thus, using the MgB<sub>2</sub>-driving body allows not only to accelerate the reactor-scaled targets to the required injection velocities, but also to provide the system performance without exceeding the acceleration limits at 500 g. As one can see from the **Table 3**, the MgB<sub>2</sub> coils (with parameters  $2\pi R_{SC} = 24$  mm,  $B_0 = 0.25$  T,  $J_C = 5000$  A) yield  $V_{inj} = 200$  m/s at 400 g on the acceleration length of 5 m.

Note that several important aspects related to a practical engineering are as follows:

- In our study, we have proposed the PMG configuration allowing in-space equilibrium position of the HTSC-sabot during its acceleration (it goes along a whole magnetic track with the same levitation height and orientation).
- Taking into account that experimentally the HTSC-sabots keep their speed after acceleration pulse, they can be extra accelerated by using a multiple-stage accelerator.
- Superconducting cables can be used not only in the driving body but also in the field coils. If these coils carry a current, which is less than the critical current, then large magnetic fields can be generated without heat generation.
- In our model, the MgB<sub>2</sub>-driving body represents a magnetic dipole (MD). The MD acceleration is carried out by a traveling magnetic wave or ARP at the consecutive switch of the field coils. From the view point of a relative positioning of the ARP and MD, the steady case is realized when the ARP pushes the MD but does not pull it for itself, that is, the area of a phase (longitudinal) stability is on a forward slope of the ARP [31]. In the accelerating equipment, it is referred to as a principle of automatic phasing. This principle will be inherent for the MgB<sub>2</sub>-driving body, because, as a superconductor, it will be pushed out from the area of a stronger magnetic field.

Especially, note that the injection velocities  $V_{inj} \geq 200$  m/s are not a problem for the proposed noncontact schedule of the target delivery. It can successfully be used in creation of a hybrid accelerator for future IFE power plants.

#### 4. Target protection system

Target delivery into IFE power plant requires target acceleration (accompanied with mechanical and thermal loads) and repeatable injection into the reaction chamber (additional thermal loads). For this reason, the problem of using the cryogenic targets in the IFE experiments or in a future reactor includes not only an issue of fabricating the qualitative cryogenic fuel layer (nonuniformity  $<1\%$ , roughness  $<1\ \mu$ ), but also an issue of target delivery at the laser focus under conditions of the layer parameter survival. In our study, a number of protection techniques have been proposed and examined with the aim of risk minimization in the process of target acceleration and injection.

A promising direction for survivability of fuel layers is application of external target protective coatings, which reduce the risks of the fuel damage under the radiation exposure from the hot walls of the reaction chamber: cryogenic coatings (from the solid  $D_2$ ,  $H_2$ , or  $Xe$ ), metal coatings from Au, Pt, Pd, and their alloys, application of a double protection: “metal + cryogenic” (**Figure 16a**). Below, we demonstrate the practical possibilities of this direction.

To obtain the results in **Figure 16b**, an additional procedure is added in the FST formation cycle. First, the metal coating made from Pt/Pd is deposited on the CH-shell. Then, the shell is filled with the  $D_2$  gaseous fuel with 3% Ne as doping agents. The next step is  $D_2$  layer fabrication by the FST layering method.

The sabot is also a special element of the target protection system [12]. An important feature of its design is the shape of a target nest. Our study shows that a proper choice of the nest shape makes it possible to significantly increase the upper limit of the permissible overloads and to minimize the injector size. Being based on the discrete-continuous physical model of the shell stress, a simulation code SPHERA is developed that makes it possible to define the stress and deformation arising in the target during the acceleration. A shape analysis of the sabot bottom (in the target nest area) during the target acceleration is carried out for three sufficiently different cases: (1) flat bottom, (2) semispherical bottom with  $R_n > R_t$  ( $R_n$  and  $R_t$  are the nest and the target radii, respectively), and (3) conical bottom (**Figure 7**). Important conclusions followed from these calculations are listed below:

- Permissible target overloads for a flat bottom are 50 times smaller than those for semispherical supports with clearance less than  $5\ \mu\text{m}$ ; at clearance higher than  $20\ \mu\text{m}$ , the stresses growing in the target are close to those of the flat bottom.
- Use of a conical bottom with the angle in cone basement equal to  $87^\circ$  provides a 20-times increase of the permissible overloads; technologically, the conical bottom has much better predictive estimate than the semispherical one.

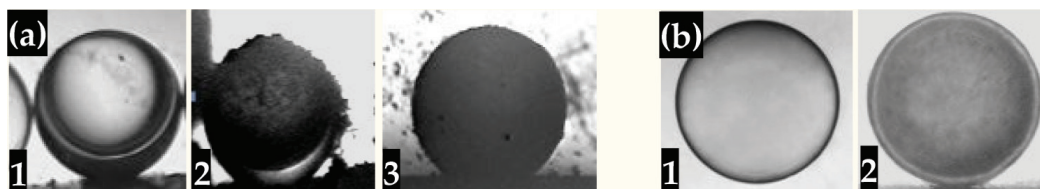


**Figure 16.**

Different protective coatings. In (a): double protection “Pd-coating of  $150\ \text{\AA}$  thick and cryogenic  $O_2$ -coating”: 1—1.2-mm CH-shell at 14.6 K before the experiment (liquid  $H_2$  inside as temperature indicator), 2—in the top part of the shell (from the outside), there is a solid deposit of oxygen ( $T_{lv} = 54.3\ \text{K}$ ), 3—after operation of the piezoelectric vibrator [22], the oxygen snow becomes redistributed onto the outer shell surface; in (b): single protection “Pt/Pd-coating of  $200\ \text{\AA}$  thick”: 1—1.5-mm CH-shell before the experiment, 2—cryogenic target at 5.0 K with a uniform  $D_2$  layer of  $50\ \mu\text{m}$  fabricated by the FST-layering method.

The next step is a shield (or cover) for application to protect injected target from a head wind of a residual gas. It has been considered since 1982 [32]. In [16], we have proposed a new design of a protective cover made from solid xenon or deuterium. At the current research stage, we have analyzed the cover and the target interaction with the reactor chamber environment using the direct simulation Monte Carlo (DSMC) approach as well as using the results of numerical studies of gas flow interaction with bodies. The following relations were considered:

- motion equation

$$L = Ut - F_D t^2 / 2M_b, \quad (5)$$

- velocity in a laminar circular wake behind the cover [33]:

$$u(x, y) = U[(\pi C_D)/32] \cdot [(2R/x)RF_D] \exp(-\eta^2), \quad (6)$$

- drag force equation for a sphere [34]:

$$F_D = -(3/4)a^2 nu(m_g k_B T / 2\pi)^{1/2} F_1 \mathbf{k}. \quad (7)$$

Here  $F_1 = F_{1o} + F_{1p}$ ,  $F_{1o} = 8\pi(8 + \pi)/9$ ,  $F_{1p} = -21.28/\xi^2$  (for two equal spheres),  $\mathbf{k}$  is the unit vector in a target motion direction,  $L$  is the distance between the body (target or cover) and the burn area,  $R$  is the characteristic dimension (target or cover),  $t$  is the in-flight time,  $F_D$  is the drag force,  $M_b$  is the mass (target or cover),  $U$  is the injection velocity,  $u(x, y)$  is current velocity,  $\eta$  and  $\nu$  are the dynamic and kinematic viscosities of a residual gas,  $M$  is the Mach number,  $m_g$  is the mass of residual gas,  $a$  is the sound speed in gas,  $k_B$  is the Boltzmann constant,  $F_{1o}$  and  $F_{1p}$  are the dimensionless drag coefficients,  $\xi$  is the dimensionless distance measured in target radii, and  $C_D$  is the coefficient of gas molecule accommodation by the target surface. The following parameters are used in our estimations: velocity is 250 m/s, residual gas is Xe at 0.5 Torr, reactor chamber radius is 5 m, cylindrical cover from solid Xe with a mass of 87 mg, and target mass is 5 mg (CHGT).

In the drag force estimations, two cases were considered: solitary and joint flight of target and cover. Correction for the solitary case (effect of wake) is about 30%. The estimations show that due to the drag force action, the distance between the target and the cover rises from the initial 1 mm at the moment of injection up to 15 mm at the center of reaction chamber. Thus, the drag force provides necessary separation of the cover and target inside the reaction chamber. The protective cover forms a wake region (**Figure 17a**) with reduced flow velocity and temperature and effectively reduces the gas heat flow by a factor of 4÷5, which is in a good agreement with calculations in [35]. Thus, the concept of protecting the direct drive target in the reactor chamber by a cover moving ahead can be considered as a possible way of solving the target delivery problem.

Note that the problem of target survival is the more difficult the higher the target temperature at the moment of injection. Estimations show that radiation heat flow from the chamber wall is an order of magnitude higher than the gas heat transfer (**Figure 17b**). Therefore, target injection at 5 K is more preferable than at 17 K. This can be realized only with an ultrafine fuel structure [1] because the single crystalline fuel reveals undesirable roughness on target cooling [2].

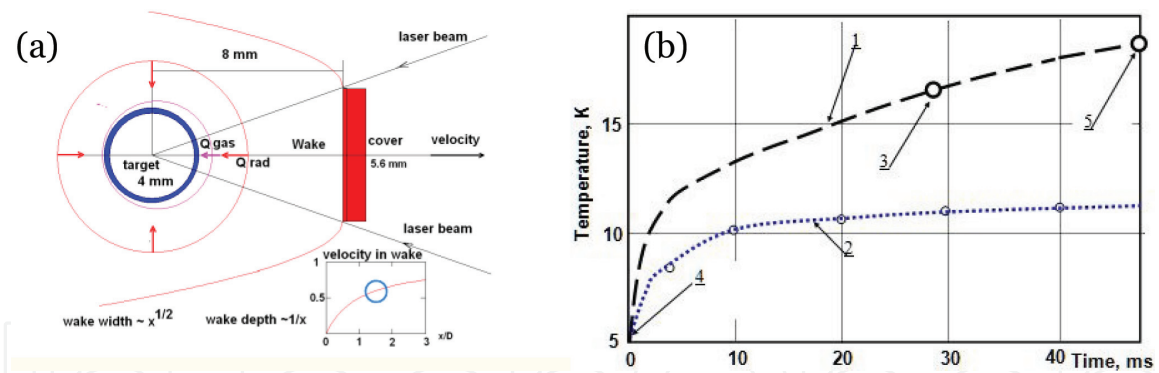


**Figure 17.** Protective cover: (a) protective cover forms a wake area in the fill gas to protect a target from the head wind and to avoid the convective heating; (b) target thermal history in IFE chamber under exposure of the wall radiation and gas convection: 4-mm targets with  $D_2$  fuel ( $200\ \mu\text{m}$ ), reactor wall temperature is 1773 K, residual gas Xe – 0.5 Torr (1—target without reflecting layer, 2—target with reflecting layer, 3— injection at 17 K, 4— injection at 5 K, 5—18.5 K, point of destination).

Basing on these results as well as on the results presented in Sections 2 and 3, we propose a multiple target protection system for the effective delivery of a cryogenic target without its damage.

1. Cryogenic layer formation with an isotropic ultrafine fuel structure (which can be referred to as layers with inherent survival features) to reduce the target sensitivity to the external thermal and mechanical loads.
2. Use of friction-free acceleration of the “HTSC-sabot + target” assembly to reduce the heat flux on the target under development of a noncontact delivery system with linear or circular accelerators.
3. Use of conical supports for a target nest in the sabot to reduce the mechanical loads during acceleration of the “HTSC-sabot + target” assembly.
4. Use of outer coatings (cryogenic, metal) in the target design to reduce risks of cryogenic layer damage as a result of target heating by thermal radiation of the hot chamber walls.
5. Coinjection of a target and a protective cover from frozen gases ( $D_2$ , Xe) to reduce risks of cryogenic layer damage as a result of target heating by hot residual gases in the reaction chamber.

The important remaining factors of the research include issues of complex technology optimization and system integration.

## 5. Conclusion

The purpose of this work was to study a repeatable target production and methods of their noncontact delivery in accordance with the scope of MM-IFE program. Various physics and technology problems accompanying IFE target-fueling development were considered, and approaches to their solution were proposed and experimentally tested partially. Our thermal, mechanical, and levitation modeling (theoretical and experimental) are important tools in planning future experiments on MM-IFE and studying IFE reactor fueling.



A particular interest from scientific and technological points of view in IFE progress deals with a cryogenic target that could be delivered to the center of reaction chamber at significant rates. Therefore, our study is devoted to the IFE target fabrication with focusing on methods, which provide a high rep-rate and cost-effective target production. The top-level requirements necessary to achieve successful target fabrication and injection deal with target material selecting and fuel layer structuring. The following issues are of key importance:

1. For target mass-production those are:

- Target materials must satisfy a wide range of required and desirable characteristics because the optimal microstructural design and material selection do allow one to obtain chemical, physical, and mechanical characteristics for specific applications.
- Target fabrication capabilities and technologies must take into account the structure particularities of the solid structure of fusion fuel.
- Fusion fuel must have an adequate thermal and mechanical stability for their quality survival in the process of target acceleration and delivery to the reaction chamber.

2. For cost-effective target production those are:

- Minimization of time and space for all production steps.
- Moving targets cooperate all production steps in the FST transmission line that is considered as a potential solution of passing from one-of-a-kind techniques to about 1 million targets per day.
- Moving targets are the necessary condition for realizing a repeatable target production at required rates and their noncontact delivery at the laser focus.

3. For survivability of a fuel core (cryogenic layer) those are:

- Layers with inherent survival features (fuel layer structuring—the grain size should be scaled back into the nanometer range).
- Noncontact delivery system.
- Multiple target protection methods including: (a) outer protective cryogenic layers, (b) metal coatings of different configurations and compositions, (c) nanocoatings for specific applications, and (d) coinjection of a special protective cover ahead of the target, etc.

For the IFE, all techniques must be integrated into an FST transmission line capable of producing about 1 million targets per day. Therefore, further studies are needed on MM-IFE connected to guide other R&D programs and to predict the behavior of IFE targets during their layering, delivery, and transport through the chamber environment. In addition, the MM-IFE allows reducing the cost of developments because it is intended to test the reactor-scaled technologies and to identify

key issues for IFE commercialization. Implementation of MM-IFE program will be useful for working-out and substantiating the technical requirements needed for creation of a laser energy power plant.

## Acknowledgements

This work was supported by the RF State Task of the Lebedev Physical Institute of Russian Academy of Sciences, and by the International Atomic Energy Agency (Research Contracts No. 20344, 11536, 13871).

## Author details


Irina Aleksandrova<sup>1</sup>, Elena Koresheva<sup>1\*</sup>, Evgeniy Koshelev<sup>1</sup>, Boris Kuteev<sup>2</sup> and Andrei Nikitenko<sup>1</sup>

<sup>1</sup> Lebedev Physical Institute of the RAS, Moscow, Russia

<sup>2</sup> National Research Center “Kurchatov Institute”, Moscow, Russia

\*Address all correspondence to: [elena.koresheva@gmail.com](mailto:elena.koresheva@gmail.com)

## IntechOpen

© 2018 The Author(s). Licensee IntechOpen. This chapter is distributed under the terms of the Creative Commons Attribution License (<http://creativecommons.org/licenses/by/3.0>), which permits unrestricted use, distribution, and reproduction in any medium, provided the original work is properly cited. 

## References

- [1] Aleksandrova I, Koresheva E. Review on high rep-rate and mass-production of the cryogenic targets for laser IFE. *High Power Laser Science and Engineering*. 2017;**5**(2). e11(1-24)
- [2] Fleurot N et al. The Laser Mégajoule (LMJ) project dedicated to inertial confinement fusion: Development and construction status. *Fusion Engineering and Design*. 2005;**74**(1):147-154
- [3] Aleksandrova I et al. Mechanical mockup of IFE reactor intended for the development of cryogenic targets mass production and rep-rate delivery into the reaction chamber. In: 27th IAEA Fusion Energy Conference: Conference Proceedings, October 22–27, 2018, Mahatma Mondir Conference Center, Ahmedabad, India
- [4] Koresheva E et al. HTSC maglev systems for IFE target transport applications. *Journal of Russian Laser Research*. 2014;**35**(2):151-168
- [5] Aleksandrova I et al. Using HTSC-band of second generation for cryogenic transport of IFE targets. *Bulletin of the Lebedev Physics Institute*. 2015;**42**(11): 309312
- [6] Aleksandrova I et al. A possibility to create the contact-free delivery system to transport the cryogenic hydrogen fuel for IFE power plants. *Bulletin of the Lebedev Physics Institute*. 2016;**43**(5): 160-166
- [7] Aleksandrova I et al. Development of hybrid transport systems for delivering cryogenic fusion targets into focus of high-power laser system or ICF reactor. *Journal of Russian Laser Research*. 2017; **38**(3):249-264
- [8] Aleksandrova I et al. Magnetic acceleration of the levitating sabot made of type-II superconductors. *Journal of Russian Laser Research*. 2018;**39**(2): 140-155
- [9] Aleksandrova I et al. Progress in the development of tomographic information processing methods for applications to ICF target characterization. *Fusion Technology*. 2000;**38**(2):190-205
- [10] Aleksandrova I et al. An efficient method of fuel ice formation in moving free standing ICF/IFE targets. *Journal of Physics D: Applied Physics*. 2004;**37**(8): 1163-1178
- [11] Koresheva E et al. Possible approaches to fast quality control of IFE targets. *Nuclear Fusion*. 2006;**46**: 890-903
- [12] Aleksandrova I et al. Cryogenic hydrogen fuel for controlled inertial confinement fusion (cryogenic target factory concept based on FST-layering method). *Physics of Atomic Nuclei*. 2017;**80**(7):1227-1248
- [13] Tretyakov Y, Oleynikov N. Synthesis of functional nanocomposites based on solid-phase nanoreactors. *Russian Chemical Reviews*. 2004;**73**(9): 974-998
- [14] Wanner R, Meyer H. Velocity of sound in solid hexagonal close-packed H<sub>2</sub> and D<sub>2</sub>. *Journal of Low Temperature Physics*. 1973;**11**(5/6):715-744
- [15] Aleksandrova I et al. Rapid fuel layering inside moving free-standing ICF targets: Physical model and simulation code development. *Laser and Particle Beams*. 2002;**20**:13-21
- [16] Aleksandrova I et al. Survivability of fuel layers with a different structure under conditions of the environmental effects: Physical concept and modeling

results. *Laser and Particle Beams*. 2008; **26**(4):643-648

[17] Aleksandrova I et al. Thermal and mechanical responses of cryogenic targets with a different fuel layer anisotropy during delivery process. *Journal of Russian Laser Research*. 2008; **29**(5):419-431

[18] Aleksandrova IV et al. FST-technologies for high rep-rate production of HiPER scale cryogenic targets. *Proceedings of SPIE*. 2011; **8080**. 80802M (1-15)

[19] Aleksandrova I et al. Ultra-fine fuel layers for application to ICF/IFE targets. *Fusion Science and Technology*. 2013; **63**:106-119

[20] Aleksandrova I et al. Pilot target supply system based on the FST technologies: Main building blocks, layout algorithms and results of the testing experiments. *Plasma and Fusion Research*. 2013; **8**(2), 3404052:1-4

[21] Osipov I et al. A device for cryotarget rep-rate delivery in IFE target chamber. In: Tanaka K, Meyerhofer D, Meyer-ter-Vehn J, editors. *Inertial Fusion Science and Applications, State of the Art 2001*. Paris: Elsevier; 2002. pp. 810-814

[22] Aleksandrova I et al. Ultra-fine hydrogen layer fabrication in the conditions of out-vibrating influence on a cryogenic target. *Voprosy Atomnoi Nauki i Tehniki. Seriya: Termoyadernyi Sintez*; 2017; **40**(3):49-62 (in Russian)

[23] Sater J et al. Cryogenic DT-Fuel Layers Formed in 1 mm Spheres by Beta-Layering. *Fusion Technology*. 1999; **35**:229-233

[24] Bodner S et al. High Gain Target Design for Laser Fusion. *Physics of Plasmas*. 2000; **7**(6):2298-2301

[25] Landau L, Lifshitz E. *Theoretical Physics. Electrodynamics of Continuous Media*. Oxford, United Kingdom: Pergamon Press; 1960

[26] Lee S et al. Development and production of second generation high Tc superconducting tapes at SuperOx and first tests of model cables. *Superconductors Science and Technology*. 2014; **27**(4), 044022:1-9

[27] Urman Yu et al. On the levitation of diamagnetic bodies in the magnetic field. *Technical Physics (Zhurnal Tekhnicheskoi Fiziki)*. 2010; **80**(9):25-33 (in Russian)

[28] Kislyak I et al. Investigations of superconductivity in MgB<sub>2</sub> bulk and Fe (steel)/MgB<sub>2</sub> wires. *Voprosy Atomnoi Nauki i Tehniki. Series: Vacuum, Pure Materials, Superconductors*. 2009; **18**: 107-110 (in Russian)

[29] Antonov Yu, Zaytsev A. *Magneto Levitation Transport Technology*. Moscow, Russian Federation: FIZMATLIT publishing house; 2014 (in Russian)

[30] Goldacker W et al. High transport currents in mechanically reinforced MgB<sub>2</sub>wires. *Superconductor Science and Technology*. 2001; **14**(9):783-793

[31] Dolya S. Acceleration of magnetic dipoles by a sequence of current-carrying turns. *Technical Physics*. 2014; **59**(11):1694-1701

[32] Frank T, Pendergrass J. Power plant design for inertial confinement fusion: Implications for pellets. *Journal of Vacuum Science and Technology*. 1982; **20**(4):1381-1386

[33] Schlichting H. *Boundary-Layer Theory*. 7th ed. New-York, USA: McGraw-Hill, Inc.; 1979. ISBN: 0070553343



[34] Gophinath A, Koch D.  
Hydrodynamic interactions between  
two equal spheres in highly rarefied gas.  
Physics of Fluids. 1970;**11**:2772-2787

[35] Valmianski E et al. Wake shields for  
protection of IFE targets during  
injection. Fusion Science and  
Technology. 2003;**43**(3):334-338

IntechOpen

IntechOpen